Fuelbreak effectiveness against wind-driven and plume-dominated fires: a 3D numerical study

Nicolas Frangieh, Gilbert Accary, Jean-Louis Rossi, Dominique Morvan, Sofiane Meradji, Thierry Marcelli, François-Joseph Chatelon

Fuelbreak effectiveness against wind-driven and plume-dominated fires: A 3D numerical study

Nicolas Frangieh [a], Gilbert Accary [b], Jean-Louis Rossi [a], Dominique Morvan [c,*], Sofiane Meradji [d], Thierry Marcelli [a], François-Joseph Chatelon [a]

[a] UMR CNRS SPE 6134, Université de Corse, 20250, Corte, France
[b] Scientific Research Center in Engineering, Lebanese University, Museum, 1106, Beirut, Lebanon
[c] Aix-Marseille Univ, CNRS, Centrale Marseille, M2P2, Marseille, France
[d] IMATH Laboratory, EA 2134, Toulon University, 83160, Toulon, France

ARTICLE INFO

Keywords:
Surface fire
Fuelbreak
Wildland fire physical model
FIRESTAR3D

ABSTRACT

The effectiveness of a fuelbreak, created in a homogeneous grassland on a flat terrain, was studied numerically. The analysis relies on 3D numerical simulations that were performed using a detailed physical-fire-model (FIRESTAR3D) based on a multiphase formulation. To avoid border effects, calculations were carried out by imposing periodic boundary conditions along the two lateral sides of the computational domain, reproducing that way a quasi-infinitely long fire front. A total of 72 simulations were carried out for various wind speeds, fuel heights, and fuelbreak widths, which allowed to cover a large spectrum of fire behaviour, ranging from plume-dominated fires to wind-driven fires. The results were classified in three main categories: 1- "Propagation" if fire crossed the fuelbreak with a continuous fire front, 2- "Overshooting" and "Marginal" if fire marginally crosses the fuelbreak with the formation of burning pockets, and 3- "No propagation" if fire does not cross at all the fuelbreak. The ratio of fuelbreak width to fuel height, marking the "Propagation"/"No propagation" transition, was found to be scaled with Byram's convection number N_c as $75.07 \times N_c^{-0.46}$. The numerical results were also compared to an operational wildfire engineering tool (DIMZAL) dedicated to fuelbreaks dimensioning.

1. Introduction

As suggested in Ref. [1], wildland fires are a multi-scale phenomenon, whose behaviour can be analysed, at least, at three levels: flame, wildfire itself, and fire regime. Three coupled time and length scales can be associated to these three levels of observation, i.e. seconds and metres for flame, days and kilometres for wildfire and years and hundreds of kilometres for fire regimes. The direct consequence of this scale separation is that behaviour of wildland fires cannot be associated to a single fire triangle as it is the case for structure fires, but to three fire triangles, whose sides are defined as follows: (Fuel/Heat/Oxygen) at flame level, (Fuel/Weather/Topography) at wildfire level, and (Vegetation/Climate/Ignition) at fire regime level [1]. The first fire triangle can be associated to firefighting operations, the two possibilities to have an action to modify fire behaviour would be: 1- reducing the amount of combustible fuel located ahead of a fire front (mechanically, by igniting a counter-fire, or by partially blocking the pyrolysis rate by dropping chemical retardants), 2- reducing the heat released by the fire front itself (by dropping water). Unfortunately, direct attack of wildfire fronts is efficient until fire intensity does not exceed a threshold value, evaluated at around 10,000 kW m^{-1} for aerial means [2]. Considering the fact that this limit is very often exceeded, and will be more and more often in the future as a consequence of global warming (average intensities of 100,000 kW m^{-1}, with a peak value reaching 150,000 kW m^{-1} were observed in Australia during Black Saturday bushfire event in Victoria in February 2009) [3]. To illustrate how powerful a 100,000 kW m^{-1} wildfire actually is, 15 m of this wildfire front released a thermal power equal to 1500 MW, equivalent of a medium-size nuclear power plant.

In conclusion, it is generally admitted by fire safety experts that reducing wildfire hazard and their consequences on people and structures cannot be only supported by increasing firefighting means, it requires moving fire safety analysis toward the second fire triangle (Fuel/Weather/Topography). Because we cannot have any action on weather and topography, the only means of reducing the risk level, or at least the impact of a wildfire on people and structures, is to reduce fuel load [4]. Reducing fuel load can contribute to achieve various objectives: reducing the impact of a wildfire on a forest (by setting-up a strategic

* Corresponding author.
E-mail address: dominique.morvan@univ-amu.fr (D. Morvan).

Nomenclature

C_P	Specific heat (J kg^{-1} K^{-1})
D_{Fire}	Fire front depth (m)
FMC	Solid fuel moisture content (%)
g	Acceleration of gravitation (m s^{-2})
H_F	Flame height (m)
H_{Fuel}	Fuel layer depth (m)
I	Fireline intensity (kW m^{-1})
LAI	Leaf Area Index
L_F	Flame length (m)
L_{FB}	Fuelbreak width (m)
L_{FBx}	Critical fuelbreak width (m)
N_C	Byram convective number
Q_R	Radiation heat flux (kW m^{-2})
ROS	Fire rate of spread (m s^{-1})
T	Gas temperature (K)
T_F	Flame temperature (K)
U_{10}	10-m open wind speed (m s^{-1})

Greek symbols

α_S	Solid fuel volume fraction
δ_R	Extinction length scale (m)
ε	Flame emissivity
γ	Flame tilt angle
τ	Atmosphere transmissivity
σ_S	Solid fuel surface area to volume ratio (m^{-1})

fuelbreak), or on the wildland urban interface (fuelbreak, clearing), reducing potential fire intensity in a natural area (prescribed burning, clearing) or during a firefighting operation (igniting a counter fire). A fuelbreak is hundred-meter-wide area where the amount of fuel at ground level is reduced mechanically, using animals (by pasturing) or using fire (prescribed burning). This safety zone can be used both to reduce the extension of a wildfire, to ensure safety conditions for firefighters during suppression operation and also be used as escape routes. The utility of such fuel management is to reduce the intensity of a potential wildfire in a forest (to avoid that it completely burns) or near houses or structures located in a wildland urban interface (WUI) [5]. Recent catastrophic fire seasons observed in various parts of the world (Alberta Canada in 2016, Portugal in 2017, California in 2017, 2018, 2020, Greece in 2018, Australia in 2019–2020) have shown that for many reasons, the urban sprawl in the WUI, the reduction of some agricultural activities, abandonment of agricultural land, and certainly also the first manifestations of global warming, wildfire hazard and its consequences upon communities (lives lost, houses and ecosystem destruction …) constitute now a major problem that must be seriously tackled [6]. For example, Hammer et al. [7] have shown in a review paper that destructions of structures in California increased by 110% between the periods 1955–1985 and 1985–2000.

Currently, there are no absolute standards for fuelbreak widths: Green and Schimke [8] showed that fuelbreaks widths of at least 65 m were necessary under high-intensity chaparral fires; Green [4] recommended a minimum of 90 m; in Corsica, a 100-m fuelbreak width is assumed, based on experts judgment but without any scientific basis [9]; and in the USA, the Quincy Library Group proposes fuelbreaks of 400 m width [10]. Because a fuelbreak can have various objectives, its design (and particularly its width) should satisfy different constraints. One objective could be to protect combustible materials (buildings, vegetation) located in a WUI, which could be ignited from a heat flux coming from a fire front. Assuming that the interaction between the flame front and a potential target was mainly due to radiation (this point will be discussed later in the paper), many studies chose to define a dimensioning criterion based on a threshold value of radiation heat flux Q_R received by a target. For example, Cohen [11] chose a radiation heat flux of 31 kW m^{-2}, which corresponds to the ignition limit of a piece of wood that is thermally thick, exposed to this heat flux during 60 s. For thin wood samples, used to study vegetation ignition, this radiation heat flux can be lower. This approach may be called “passive fuel-breaking”. Another objective of fuelbreak, more related to firefighting activity, could be to offer to firefighters a safety zone along fire-front trajectory; in this case, the safe separation distance (SSD), i.e. acceptable safety distance between a firefighter and a fire front, must be evaluated with a lower radiative heat flux, and the recommended value in this case is 7 kW m^{-2}. Considering that a firefighter can operate in safe conditions at the middle of the fuelbreak (that should also include an access trail in this case), fuelbreak must be twice as wide as the SSD [5]. This approach may be called “strategic fuel-breaking”.

This study is dedicated to the first approach, i.e. the problem of designing a passive fuelbreak, about which only few theoretical studies exist in literature. The first paper that addressed fuelbreak effectiveness was published in 1964 by Emmons [12] who proposed a 1D simplified physical model based on the assumption that heat transfer between the fire front and vegetation was exclusively governed by radiation. Using an energy balance equation, he proposed an effectiveness criterion, given by Eq. (1), linking the fuelbreak width (L_{FB}) to Leaf Area Index (LAI) characterizing vegetation layer and fire front depth (D_{Fire}):

$$L_{FB} \geq \frac{LAI\ D_{Fire}}{2} \tag{1}$$

Green and Schimke [8], estimated that the distance from a wildfire required to prevent ignition by radiation was half the distance required to prevent disabling burns. As strategic fuelbreaks must act as barriers to stop or slow down a fire spread and must also form safety zones where firefighters and their equipment can retreat to escape injury [5], the SSD concept is also used to assess fuelbreak widths. The SSD is the distance between firefighters and fire required to prevent firefighters' injuries. So, assuming that fuelbreak center is a safety zone, total width of a fuelbreak should theoretically be at least twice as large as the SSD [13, 14]. The analytical model proposed by Rossi et al. [13] and implemented in an operational tool “DIMZAL” was based on radiative heat flux threshold of 7 kW m^{-2} that an equipped firefighter would withstand without being injured. The distance at which this threshold heat flux Q_R would impact a theoretical target is a function of flame-front characteristics (flame length, flame temperature, flame tilt angle …) and is given by Eq. (2) [13], where L_F is the flame length, γ is the flame tilt-angle, T_F is the flame temperature, and ε and τ are the flame emissivity and atmosphere transmissivity, σ is Stefan-Boltzmann constant, respectively.

$$SSD = L_F\left[\frac{\cos\gamma\left(\left(\varepsilon\tau\sigma T_F^4\right)^2 - 4Q_R^2\right)^{1/2}}{2Q_R} + \sin\gamma\right] \tag{2}$$

Noticing that flame height was very often equal to twice the vegetation depth, Butler and Cohen [15] had previously proposed a simpler criterion to evaluate the SSD, given by Eq. (3), based on the flame height (H_F) and on a threshold heat flux equal to 7 kW m^{-2}.

$$SSD \geq 4 \times H_F \tag{3}$$

By comparing Eqs. (2) and (3), the expression proposed by Rossi et al. [13] can be considered as a generalization of the expression proposed by Butler and Cohen [15], that includes wind effect on the flame geometry. The factor 4 in Eq. (3) was replaced in Eq. (2) by a function that depends on the flame characteristics (tilt angle and flame

temperature) and on the radiative heat flux. Also, flame height in Eq. (3) was replaced in Eq. (2) by flame length to take into account the deflection of flame trajectory.

It should be noted that in order to maintain a certain aesthetical quality of landscape (in national or regional parks for example), a fuelbreak does not necessarily mean a zone in which all vegetation must be completely removed. Some trees can be preserved while maintaining some safety distance between two crowns, in a typical configuration called shaded fuelbreak [10] that has the capacity to stop fire propagation at crowns level, by maintaining fire only at understory level [16].

The purpose of the present paper is to study fuelbreak effectiveness (created on a flat terrain, to simplify the analysis) against wildland fires in different fire regimes. This study is based on numerical simulations that were performed using a 3D CFD fire model, in the continuity of a previous 2D study [17]. This preliminary 2D study highlighted the role played respectively by radiation and convection heat transfer on the capacity of a surface fire propagating through a homogeneous Mediterranean shrubland of crossing or not a fuelbreak. Because the objective of a fuelbreak is to efficiently stop fire propagation in various fire conditions, this paper proposes to generalize the preliminary 2D study [17] to a more realistic conditions, by performing 3D simulations and by covering a large spectrum of propagation regimes ranging from plume-dominated fires to wind-driven fires. Most of the existing studies on the evaluation of a fuelbreak are based on classical ignition theory [18–20]; it consists first in relating ignition time to the radiation heat flux received by a target (that can be thermally thin or thermally thick), then in evaluating a home ignition zone (HIZ) from an acceptable level of risk [13,21,22]. As underlined by previous 2D study [17], the ignition process that governs fuelbreak effectiveness, is not exclusively piloted by radiation heat transfer, sometimes this ignition can result from a convective heat transfer between hot gases coming from the plume and dry vegetation located at the fuelbreak edge. In fact, the propagation of a fire front and therefore its capacity to cross a fuelbreak, are strongly correlated to the flame and plume direction, more or less tilted by the wind flow [23]. Depending on the ratio between the two forces governing the flame trajectory, i.e. wind inertia and buoyancy, two modes of fire propagation were already identified: plume dominated and wind driven [23,24]. The vertical structure of fire front, more or less consisting of a succession of peaks and troughs, must also affect the fire front dynamics and flame/vegetation interaction [25,26]. The fact that a fire front is far to be a simple uniform radiant panel and the potential role played by convective heat transfer, justify that investigating the problem of fuelbreak effectiveness cannot be carried out by simply considering the radiation heat flux received by a potential target, but requires considering the 3D character of fire, which is the main objective in this paper.

In order to avoid superposition of parameter effects, the simplest as possible configuration was considered, by choosing a homogeneous fuel layer, a grassland on a flat terrain, cut in the middle by a fuelbreak where fuel was completely removed. To cover a large spectrum of fire behaviour, the simulations were performed by varying two parameters: the 1-m open wind speed (U_1, ranged from 3 to 14 m s^{-1}) and fuel height (H_{Fuel}, ranged between 0.25 and 1 m).

Readers should be aware that this particular choice of fuel layer (grass) may limit the generalization of the results highlighted in this study. However, because this kind of fuel is very dry, it also constitutes a good test by maximizing the level of risk (a good thing in such fire safety study). Prescribed fires are also very often performed in grasslands, which requires fuelbreaks to guaranty the safety conditions of such operations. At the end of the paper, the analysis of the results in terms of non-dimensional numbers (length ratio versus Byram's convective number), extends the study to other fuel types.

1.1. Physical and mathematical model

A set of numerical simulations was carried out for fire propagating through a homogeneous grassland, as shown in Fig. 1. In order to achieve a quasi-steady state of fire propagation before the fire front reaches the fuelbreak, computational domain dimensions were adapted according to wind speed as follows: $L_{FE} = 30$ m ($U_1 = 3$ m s^{-1}), $L_{FE} = 40$ m ($U_1 = 5$ m s^{-1}), $L_{FE} = 60$ m ($U_1 = 8$ and 10 m s^{-1}), $L_{FE} = 80$ m ($U_1 = 12$ and 14 m s^{-1}). Consequently, the domain length in the fire propagation direction L_X varied from 140 to 200 m, the domain width in transverse direction L_Y varied from 50 (for $U_1 = 3$ m s^{-1}) to 80 m (for $U_1 = 12$ and 14 m s^{-1}), while the computational domain height L_Z was fixed at 40 m. At the domain entrance, a 20 m-wide band, without any vegetation, was placed to initiate the atmospheric boundary layer. A 1/7-power vertical velocity profile was used at the domain inlet with a turbulence intensity of 10%. Tests have shown that the 20-m entrance region was sufficient to initiate the atmospheric boundary layer, and that increasing this region length has no noticeable effect on the obtained results. Vegetation was ignited using a 1 m-wide (in X direction) gaseous burner located along the entire leading edge of the vegetation layer.

Physical properties and characteristics of the solid fuel layer are detailed in Table 1. With these values, the extinction length scale δ_R characterizing heat transfer by radiation, given by Eq. (4), is equal to 0.5 m [27], where α_s is the solid fuel volume fraction and σ_s surface area to volume ratio of solid fuel particles.

$$\delta_R = \frac{4}{\alpha_S \, \sigma_S} \tag{4}$$

To respect the constraint required for a good representation of physical phenomena governing fire behaviour [27], mesh dimensions were chosen as follows:

- In the solid phase (the vegetation): $\Delta x = \Delta y = 0.25$ m and $\Delta z = 0.0125$ m,
- In the gaseous phase: $\Delta x = \Delta y = 0.5$ m and $\Delta z = 0.025$ m for z ranged between $z = 0$ and $z = 1$ m, then mesh was gradually coarsened according to a geometrical progression with a ratio = 1.04.

Notice that mesh size is always less or equal to the extinction length-scale δ_R, given by Eq. (4) and equal to 0.5 m [27]. A previous numerical study of a fire front ignited in a tube filled with pine needles had shown that this condition was sufficient to correctly reproduce the heat transfer (by radiation in this case) piloting fire front propagation and therefore to avoid any numerical artefact [28]. In addition, cold simulations of a turbulent boundary layer above a canopy performed with similar mesh sizes, had shown quite good results compared to experimental data [29]. Even if it would be preferable in LES [30] to use mesh sizes with aspect

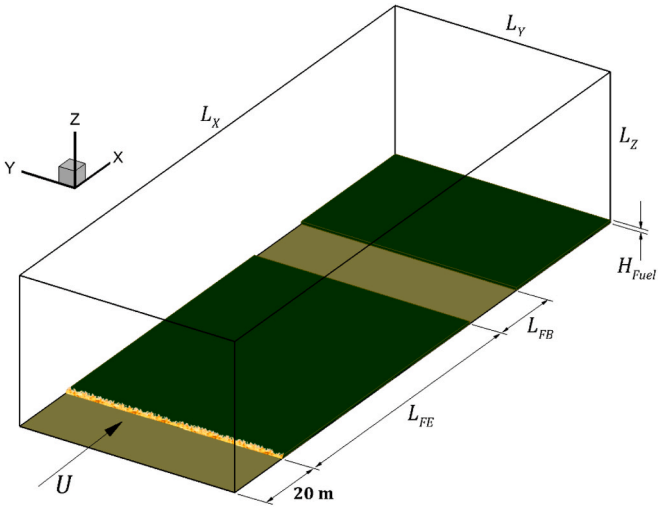

Fig. 1. Fluid-phase and solid-phase computational domains used to simulate grassland fire with a fuelbreak.

Table 1
Physical properties of the solid fuel layer.

Fuel density ρ_S (kg m^{-3})	500
Specific heat C_{PS} (J kg^{-1} K^{-1})	1380
Fuel volume fraction α_S	0.002
Fuel moisture content FMC (%)	5
Surface area to volume ratio σ_S (m^{-1})	4000
Fuel height H_{Fuel} (m)	From 0.25 to 1
Fuel load W (kg m^{-2})	From 0.25 to 1
Extinction length scale δ_R (m)	0.5
Leaf Area Index LAI (2 H_{Fuel}/δ_R)	From 1 to 4

ratios $\Delta x/\Delta z$ and $\Delta y/\Delta z$ nearly equal to unity, considering that effect of the wind flow and the vertical extension of the flame on the fire behaviour could be important, we have refined the mesh along the vertical direction (z). As a consequence of that, the mesh size near the ground and above the canopy was characterized with aspect ratios $\Delta x/\Delta z$ and $\Delta y/\Delta z$ much larger than one and equal to 20. However, the mesh size chosen along the x and y directions was considered as a compromise between reasonable computational time and acceptable accuracy [30].

As mentioned in introduction, the influence of fuel height H_{Fuel} and of wind speed U_1 (evaluated 1-m above ground level) was tested in this study. Five values of H_{Fuel} (0.25, 0.35, 0.5, 0.75, and 1 m) and six values U_1 (3, 5, 8, 10, 12, and 14 m s^{-1}) were considered. In order to relate the analysis to literature where the 10 m-open wind speed U_{10} is often used, the ratio $U_{10}/U_1 = 1.39$ for a 1/7-power inlet velocity profile. The distance L_{FE} in Fig. 1 was adapted according to the wind speed in order to obtain a quasi-steady fire-front propagation (criterion based on the value of the average rate of spread) before reaching the fuelbreak. 18 combinations of the fuel height and the wind speed were considered, and for each combination, at least three fuelbreak widths L_{FB} were tested; in total 72 simulations were carried out.

The simulations were carried out using a fully-physical fire-model (FIRESTAR3D). Because each solid fuel particle constituting the vegetation cannot be represented in detail, the problem is formulated using a multiphase approach, consisting in averaging balance equations of mass, momentum, energy, and so on, governing the coupled physical system formed by the vegetation and the surrounding atmosphere, inside control volumes containing both solid and gaseous phases. This approach was initially proposed by Grishin [31] to study forest fires, then quasi simultaneously, with some variations in the formulations, by other authors, such as Larini et al. [32], Linn [33], Morvan et al. [34]. The vegetation layer is represented as a sparse porous media (volume fraction α_S occupied by the solid phase was always less to 1%), and the averaging process of conservation equations applied to the control volumes results in the introduction of additional source/sink terms, representing the interaction between solid and gaseous phases. In momentum balance equations for example, the presence of solid fuel particles results in the addition of drag forces that contribute to the reduction of wind speed inside a forest. Other similar source/sink terms are present in mass and energy equations, reflecting the production of gases resulting from vegetation decomposition (by drying and pyrolysis) and the intense heat flux exchanged (by radiation and convection) between vegetation and surrounding atmosphere. The consequences of the turbulence characterizing atmospheric flow surrounding the flame front is taken into account in using a Large Eddy Simulation (LES) approach. Additional models are introduced to account for turbulence-combustion interaction as well as turbulence-radiation interaction. The degradation process of the solid fuel (illustrated by Fig. 2) was reproduced as follows [35]:

- Vegetation water is lost by vaporization at a constant temperature T = 373 K,
- Dry fuel is decomposed into CO, CO_2, charcoal, and soot by pyrolysis between 400 K and 500 K,

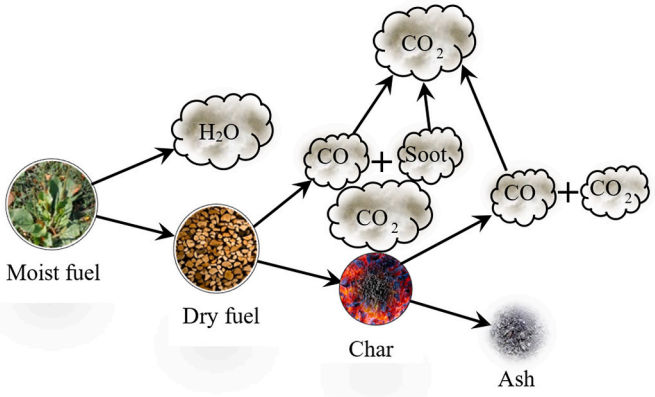

Fig. 2. Fuel degradation model (general scheme).

- Gaseous CO produced by pyrolysis burns in the gaseous phase producing CO_2,
- Charcoal undergoes complete or incomplete combustion producing a mixture CO/CO_2, CO/CO_2 ratio is a function of charcoal temperature,
- Gaseous CO released by incomplete char oxidation burns in the gaseous phase producing CO_2.

Because all model details have already been published, and in order to emphasise the physical aspects in the present paper, readers who would interested by these technical aspects are invited to consult following papers: [34–36].

It can be underlined that the use of this kind of engineering tool to evaluate the effectiveness of fuelbreaks, is limited to situations where convective and radiation heat transfers are the main sources of interaction between the fire front and a potential target. This study ignores completely the very important role played by firebrands, which sometimes represent one of the main sources of vulnerability of houses located in WUI. In this case, the objective of fuelbreaks in WUI is to allow firefighters to stay in safe conditions in the vicinity of houses to be defended [7,37].

1.2. Numerical results and discussion

The set of variable parameters (fuel height and wind speed) was duly chosen in order to analyse the fuelbreak effectiveness for different fire-propagation regimes (from plume-dominated to wind-driven). Numerical simulations were performed in such way to obtain a large interval of Byram's convective number (Eq. (5)), that nearly ranged between 0.4 and 50. This very important similarity parameter, represents the power ratio of the two forces governing the trajectory of flames and consequently the propagation of a wildfire, i.e. buoyancy force due to temperature difference (and therefore density) between the hot plume above the fire and ambient air, and inertia force due to the wind.

$$N_C = \frac{2\,g\,I}{\rho_0\,C_{P0}\,T_0\,(U_{10} - ROS)^3} \tag{5}$$

A first set of numerical results is presented in Figs. 3–6, showing the fuel bulk density ($\overline{\rho_S} = \alpha_S \times \rho_S$) at the top of the vegetation layer ($z = H_{Fuel}$). These simulations were performed for the same wind speed ($U_1 = 8$ m s^{-1}) and the same fuel load (W = 0.5 kg m^{-2}, only the fuelbreak width varied from a simulation to another one: $L_{FB} = 0$ m (no fuelbreak) (Fig. 3), $L_{FB} = 20$ m (Fig. 4), $L_{FB} = 19$ m (Fig. 5), $L_{FB} = 10$ m (Fig. 6). With these values, the Byram's convective number N_C, calculated a posteriori from Eq. (5), after evaluating the rate of spread (ROS), was equal to 4.2, this corresponds to a hybrid fire propagation regime lying between plume dominated (observed for $N_C > 10$) and wind driven (observed for $N_C < 2$) fires [38]. For each configuration, fire intensity I

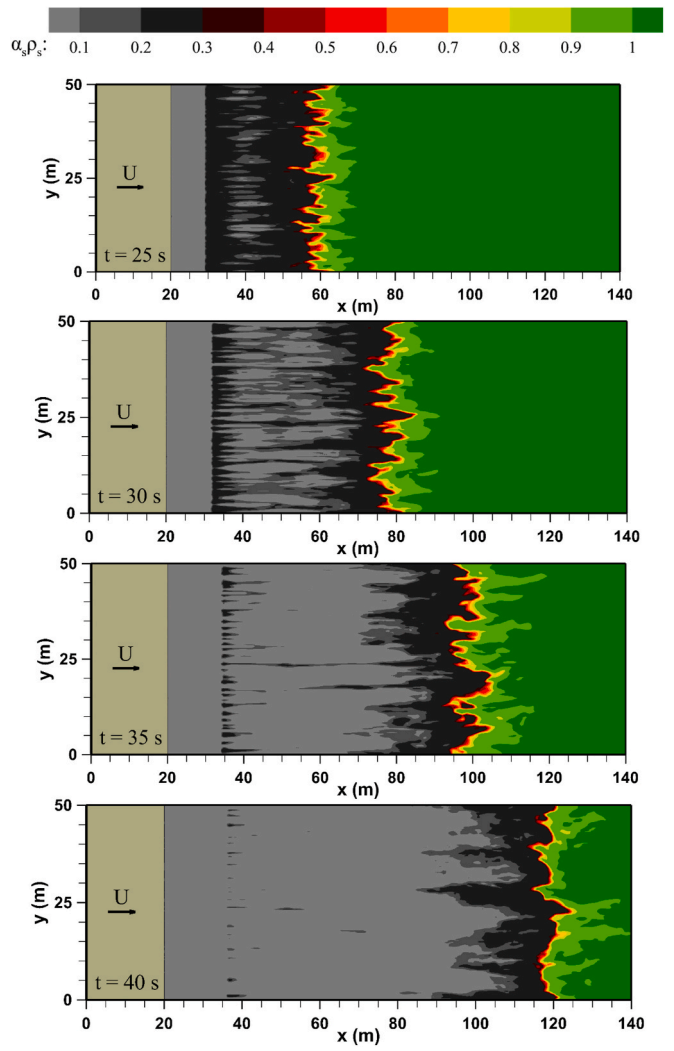

Fig. 3. Distribution of the bulk fuel density at the grassland top surface at different simulation times, for $U_1 = 8$ m s^{-1}, W = 0.5 kg m^{-2} and for the reference case (without fuelbreak) chosen to evaluate Byram's convective number (Nc = 4.2). Color code: Green (initial state fuel), Light green (dry fuel), Yellow-Red (mixed dry fuel/char), Black (char), Grey (ashes). (For interpretation of the references to colour in this figure legend, the reader is referred to the Web version of this article.)

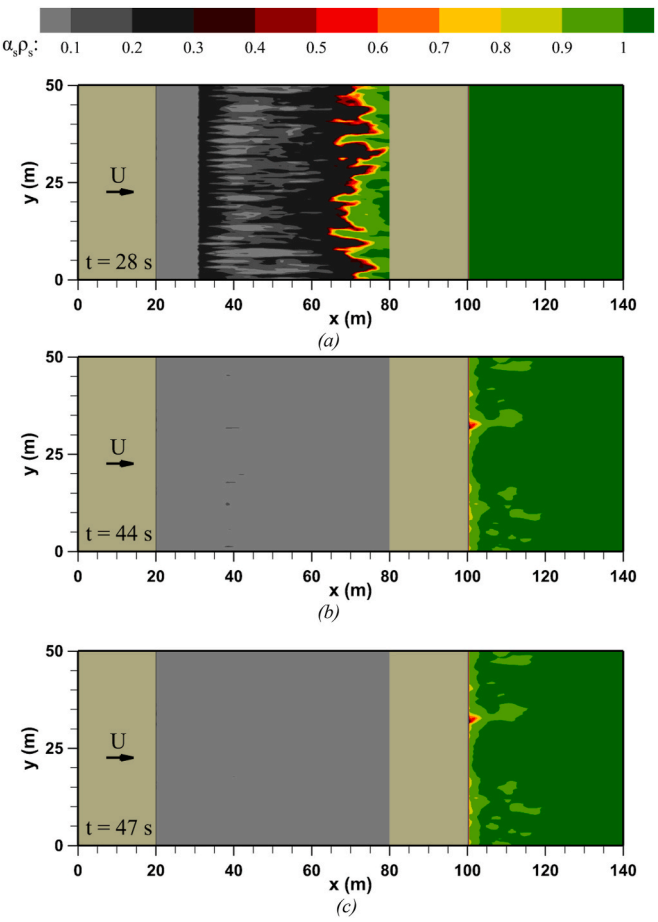

Fig. 4. Distribution of the bulk fuel density at the grassland top surface at different simulation times, for $U_1 = 8$ m s^{-1}, W = 0.5 kg m^{-2} (Nc = 4.2), and for a fuelbreak width $L_{FB} = 20$ m (No propagation). Color code: Green (initial state fuel), Light green (dry fuel), Yellow-Red (mixed dry fuel/char), Black (char), Grey (ashes). (For interpretation of the references to colour in this figure legend, the reader is referred to the Web version of this article.)

and the rate of spread ROS required to calculate Byram's convective number (Eq. (5)) were evaluated for the reference case, i.e. fire propagating through a homogeneous fuel layer (without fuelbreak), once the global behaviour of fire front had reached a quasi-steady (as shown by Fig. 3). It may be observed in Fig. 3 that the heterogeneous combustion had not really reached its full intensity at t = 30 s, as witnessed by the amount of charcoal on the back side of the fire front (black colour). Between t = 30 s and t = 35 s, a rapid expansion of the grey zone (corresponding to ash), reflecting an increase of the heterogeneous combustion rate may be noticed. The patterns are quite similar between t = 35 s and t = 40 s, indicating that the heterogeneous combustion had reached its full intensity.

In these simulations (and in all others), fuel bulk density was ranged from 1.024 kg m^{-3} (for the initial fuel state) to 0.039 kg m^{-3} (when the fuel is entirely consumed and ash state is reached). To clearly highlight the position of the fire front, six colours were used:

- Grey ($\overline{\rho_S} = 0.039\ kg\ m^{-3}$) for ashes state
- Black ($0.039 < \overline{\rho_S} \leq 0.25\ kg\ m^{-3}$) for char combustion
- Red ($0.25 < \overline{\rho_S} < 0.5\ kg\ m^{-3}$) for pyrolysis and combustion
- Yellow ($0.5 < \overline{\rho_S} < 0.75\ kg\ m^{-3}$) pyrolysis
- Light green ($0.75 < \overline{\rho_S} < 1\ kg\ m^{-3}$) for drying and pyrolysis
- Green ($\overline{\rho_S} = 1.024\ kg\ m^{-3}$) for initial fuel state

As expected, before fire reaches the fuelbreak, it globally exhibits the same behaviour as shown in Figs. 4(a), 5(a), and 6(a). Even if these three pictures correspond to the same simulation time, they are not fully identical due to the very-nonlinear nature of physical mechanisms governing the fire. This apparent artefact is also typical of Large Eddy Simulations (LES) used here to treat turbulence, it is well known that LES preserves the sensitivity to initial conditions characterizing such kind of physical system; here, small differences between Figs. 4(a), 5(a), and 6(a) are the result of truncation errors and small random perturbations applied to the initial velocity field of amplitude 0.1 m s^{-1} used to initiate turbulence. Then as the fire front reaches the fuelbreak edge, fire behaviour changes with fuelbreak width from stop and extinction for Fig. 4(b) and (c) ($L_{FB} = 20$ m) to propagation beyond the fuelbreak for Fig. 6(b) and (c) ($L_{FB} = 10$ m). The intermediate situation shown in Fig. 5 ($L_{FB} = 19$ m), called "Overshooting", represents a threshold case, for which fire can cross the fuelbreak in some points, consequently forming few burning pockets. We can also notice that even when fire crosses the fuelbreak and keeps propagating as a continuous fire front later on, the early stage of the transition is characterized by a distribution of separate burning pockets, as shown in Fig. 6 (b), that end up merging together forming again a continuous front as shown in Fig. 6 (c). We also

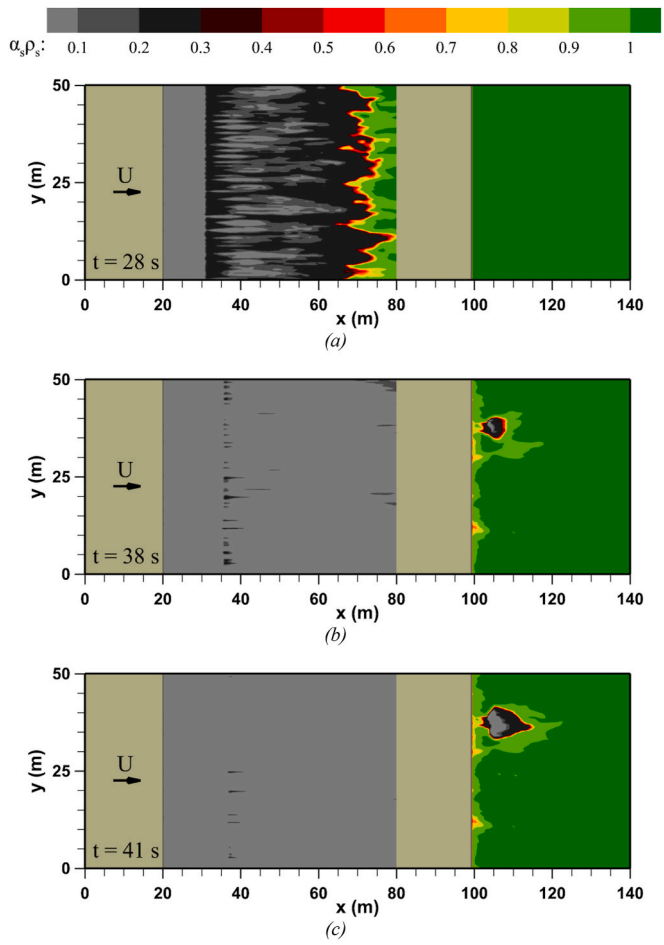

Fig. 5. Distribution of the bulk fuel density at the grassland top surface at different simulation times, for $U_1 = 8$ m s^{-1}, W = 0.5 kg m^{-2} (Nc = 4.2), and for a fuelbreak width $L_{FB} = 19$ m (Overshooting). Color code: Green (initial state fuel), Light green (dry fuel), Yellow-Red (mixed dry fuel/char), Black (char), Grey (ashes). (For interpretation of the references to colour in this figure legend, the reader is referred to the Web version of this article.)

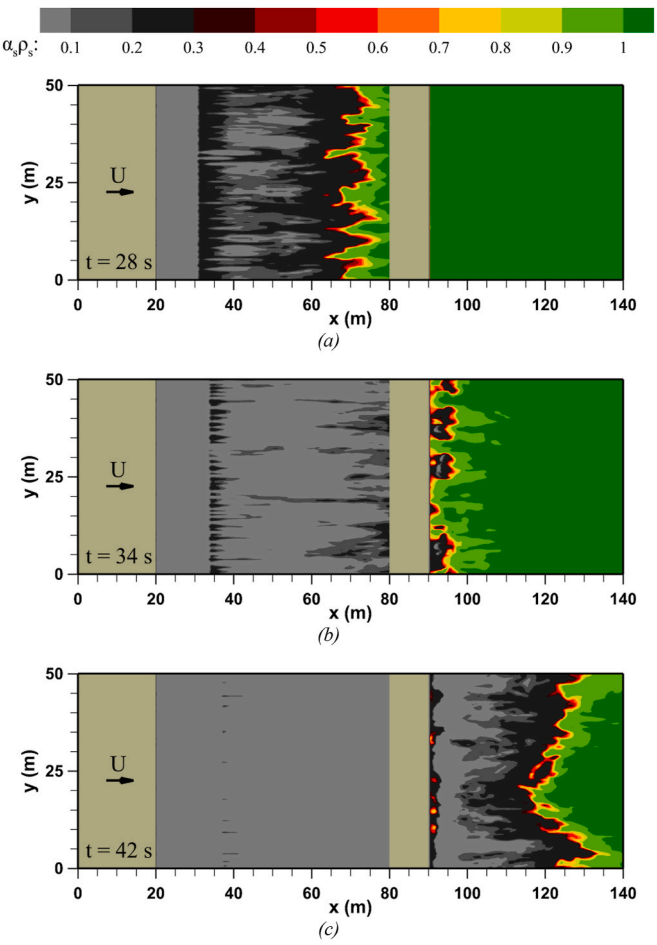

Fig. 6. Distribution of the bulk fuel density at the grassland top surface at different simulation times, for $U_1 = 8$ m s^{-1}, W = 0.5 kg m^{-2} (Nc = 4.2), and for a fuelbreak width $L_{FB} = 10$ m (Propagation). Color code: Green (initial state fuel), Light green (dry fuel), Yellow-Red (mixed dry fuel/char), Black (char), Grey (ashes). (For interpretation of the references to colour in this figure legend, the reader is referred to the Web version of this article.)

underline that the absence of vegetation in the fuelbreak contributes to locally accelerate the wind flow near the ground and at flame level as well, with the consequence that the fire front can temporarily accelerate after crossing the fuelbreak, from these burning pockets.

This scenario certainly results from the vertical structuration of the flames front in peaks and valleys [25,26] that contributes to modulate heat transfer between the flames and the unburned fuel: a peak releases more energy by radiation compared to a trough, while a trough allows hot gases to cross the fire front and heat the unburned fuel by convection.

The 3D character of fire as it crosses the fuelbreak is shown in Fig. 7 for $U_1 = 8$ m s^{-1} and $W = 0.5$ kg m^{-2} and for the three considered fuelbreak widths; subfigures correspond to Figs. 4(b), 5(b), and 6(b). The isovalue surface of gas temperature T = 1000 K is shown in yellow representing the flames, and isovalue surface of mass fraction of water vapour $Y_{H2O} = 10^{-3}$ is shown in semi-transparent grey. Even if choosing isotherm T = 1000 K to define the flame geometry might be considered as a little bit arbitrary, since the flame is located in a high temperature gradient region, we can consider that this choice should not be far from reality and it should at least not affect noticeably the results. These figures clearly highlight the differences between two typical behaviours: "Overshooting" and "Propagation". In the "Overshooting" case, we can notice that fire locally ignites a pocket of solid fuel but is unable to reconstitute a continuous fire front later on. From this point ignition, fire may have the possibility of growing again, but for some time its intensity is seriously reduced by comparison to situation observed before fire reaches the fuelbreak edge. Even in the case where fire crosses and propagates beyond the fuelbreak, it takes some time (about 10 s in this case) before recovering its initial intensity, as we can notice in Fig. 8 showing the time evolution of the heat release rate (HRR) (Fig. 8(a)) and the pyrolysis front trajectory (Fig. 8(b)) for $U_1 = 8$ m s^{-1} and $W = 0.5$ kg m^{-2} in three configurations: with and without a 10 m and 19 m wide fuelbreak. In our study, HRR was evaluated from Eq. (6), including a positive contribution of the energy released by homogeneous combustion of CO in the gaseous phase and by heterogeneous combustion of char and soot, and a negative contribution of the energy absorbed by pyrolysis and vaporization [26].

$$HRR = \dot{\omega}_{CO} \cdot H_{CO} + \dot{\omega}_{Char} \cdot H_{Char} + \dot{\omega}_{Soot} \cdot H_{Soot} - \dot{\omega}_{Pyr} \cdot H_{Pyr} - \dot{\omega}_{Vap} \cdot H_{Vap} \quad (6)$$

We can notice in Fig. 8(a) relatively large fluctuations of the HRR, which could result from the relatively complex energy balance evaluated globally in the whole computational domain (Eq. (6)). However as shown by Fig. 8(b), this does not seem to noticeably affect the fire front behaviour, since the time evolution of the pyrolysis front position does not exhibit the same unsteady behaviour, it exhibits on the contrary a quasi-linear behaviour when the fire front reaches the fuelbreak.

Consequently, from these results, we can partially conclude (at least

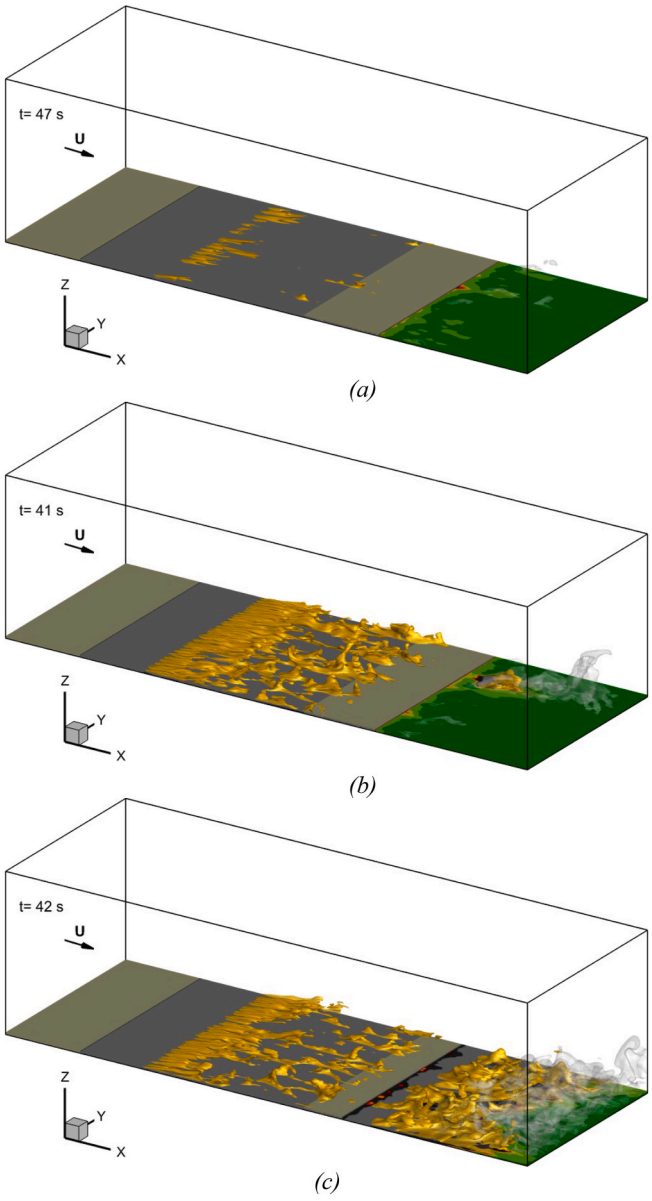

Fig. 7. 3D visualisation of grassland fire with fuelbreak obtained for $U_1 = 8$ m s^{-1}, W = 0.5 kg m^{-2} (Nc = 4.2), and for three values of the fuelbreak width. (a) L_{FB} = 20 m (No propagation), (b) L_{FB} = 19 m (Overshooting), (c) L_{FB} = 10 m (Propagation). The yellow surface is the isovalue surface T = 1000 K of the gas temperature and the semi-transparent grey surface is the isovalue surface Y_{H2O} = 10^{-3} of the mass fraction of water vapour. (For interpretation of the references to colour in this figure legend, the reader is referred to the Web version of this article.)

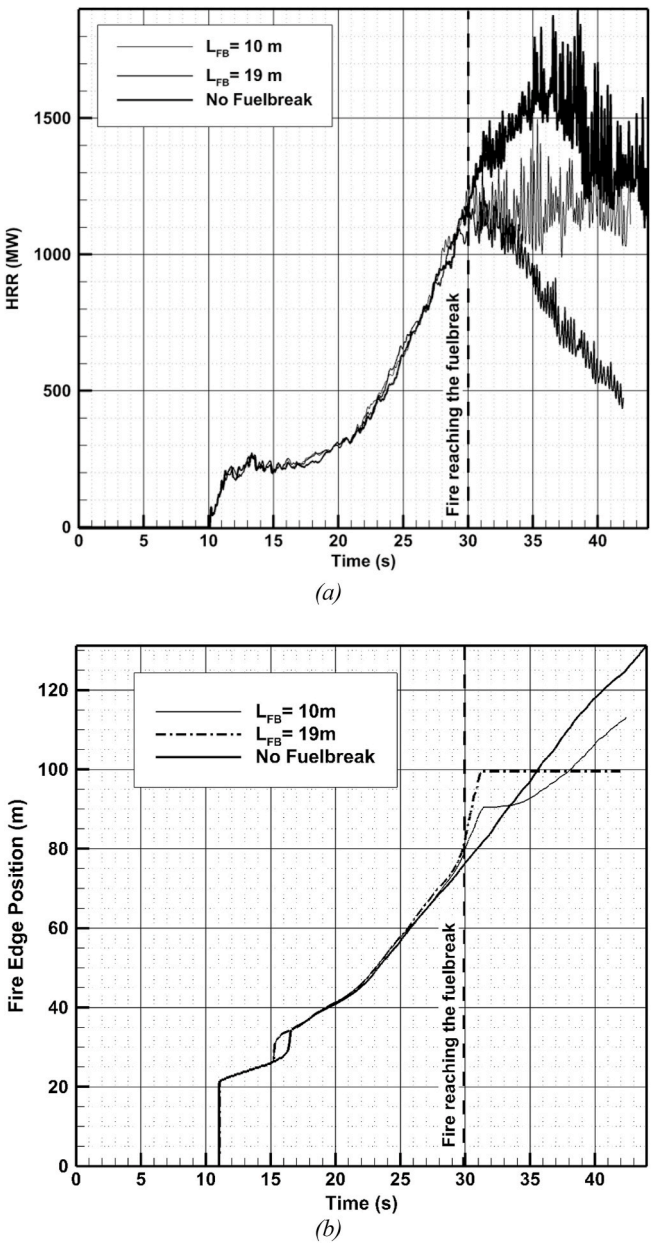

Fig. 8. Time evolution of the heat release rate (HRR) (a) and trajectory of the pyrolysis front (b) obtained for $U_1 = 8$ m s^{-1} and W = 0.5 kg m^{-2} (Nc = 4.2), with and without a fuelbreak.

for this configuration) that, in cases where fire succeeds in crossing the fuelbreak (both for 10 m and 19 m width), because the fire intensity decreases during a certain period of time, it could be theoretically treated (held back or suppressed) by firefighters (if safety conditions are satisfactory). In the case of 19-m wide fuelbreak, based on the HRR decrease in Fig. 8(a), fire could stop or could at least reach a sufficiently low intensity level to be suppressed by firefighters.

Time evolution of the heat rate density absorbed by radiation and convection with a vegetation particle located at position (X = 90 m, Y = $L_Y/2$, Z = H_{Fuel}), i.e. on the median plane and at the top of solid fuel layer, is shown in Fig. 9 in the absence of a fuelbreak. Time evolution of particle temperature at the same point is also reported. The vertical dashed line indicates time at which vegetation temperature reaches 500 K; this corresponds to value at which pyrolysis rate reaches its maximum level. As vegetation temperature reaches the threshold value of 500 K, we can notice that the energy received by the vegetation top by convection (210 kW m^{-2}) is more than four times the amount of energy received by radiation (50 kW m^{-2}). Even if Byram's convective number characterizing the free propagation of fire (N_C = 4.2) is larger than the theoretical value (N_C = 2) under which fire propagation is essentially wind driven fire regime is supposed to be reached (for these case N_C = 4.2), Fig. 9 indicates that fire propagation is mainly governed first by convection during pyrolysis phase, then by radiation as the solid fuel is ignited.

In order to explore other propagation regimes, we also present the two following cases:

- A fuel load $W = 0.5$ kg m^{-2} and a wind speed $U_1 = 3$ m s^{-1}, resulting in a Byram's convective number N_C = 23,

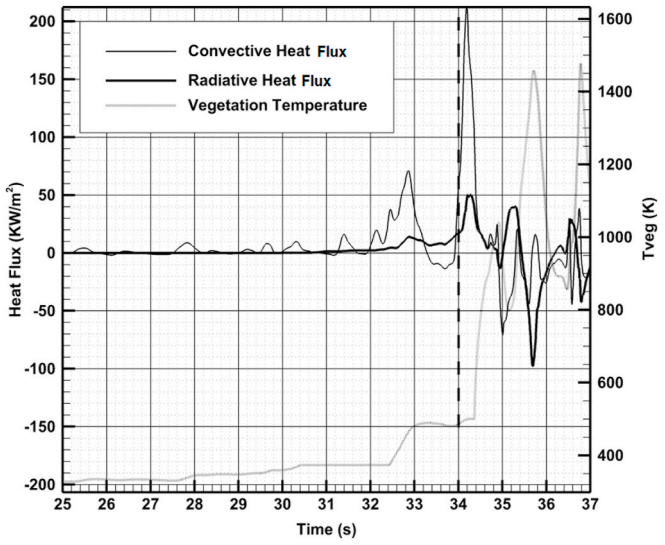

Fig. 9. Time evolution of the radiative and the convective heat fluxes received by a vegetation particle located at point (90 m, $L_Y/2$, H_{Fuel}) and of the corresponding particle temperature, obtained without fuelbreak for $U_1 = 8$ m s^{-1} and W = 0.5 kg m^{-2} (Nc = 4.2).

- A fuel load $W = 0.35$ kg m^{-2} and a wind speed $U_1 = 8$ m s^{-1}, resulting in a Byram's convective number $N_C = 1.95$.

These two cases were chosen in order to target both plume dominated regime ($N_C > 10$) and wind driven one ($N_C < 2$) before fire front reaches the fuelbreak. Figs. 10 and 11 show results obtained in the first case for two fuelbreak widths: $L_{FL} = 8$ m and $L_{FL} = 6$ m respectively. Fig. 10 illustrates again an "Overshooting" case, with a fire able to locally cross the fuelbreak but without enough intensity to continue its propagation beyond the fuelbreak. In return, Fig. 11 shows how multiple burning pockets ignited after the fuelbreak allow fire to continue its propagation beyond this obstacle.

Same numerical experiment was carried out for a wind driven fire and the results are shown in Fig. 12 (for $L_{FB} = 17.5$ m) and Fig. 12 ($L_{FB} = 6.5$ m). Again, the results clearly illustrate the necessary mechanism for a fire to cross a fuelbreak, i.e. the necessity of multiple ignition points, close enough to have the possibility to merge and to reconstruct a continuous propagating fire front. As for the first set of numerical results ($N_C = 4.2$), the question of the dominant heat transfer mode ahead of the fire front is addressed in Fig. 14. In the case of plume dominated fires (Fig. 14(a), $N_C = 23$) heat exchanges between the flame and unburned fuel during preliminary heating phase (drying and pyrolysis), were always dominated by convection (130 kW m^{-2}), compared to the contribution of radiation which stayed approximately at the same level (50 kW m^{-2}). Then during ignition phase, both convection and radiation seem to equally contribute as shown by Fig. 14(a). In wind driven fire case (Fig. 14(b), $N_C = 1.95$), the difference of contribution between convection and radiation is less marked, and both modes of heat transfer seem to balance out, with a little advantage for heat transfer by convection. A preliminary conclusion that we can extract from these results is that in 3D, the dominance of heat transfer by convection in 3D simulations, at least during preheating phase (drying and pyrolysis) is more pronounced by comparison to what it was observed in 2D simulations [39].

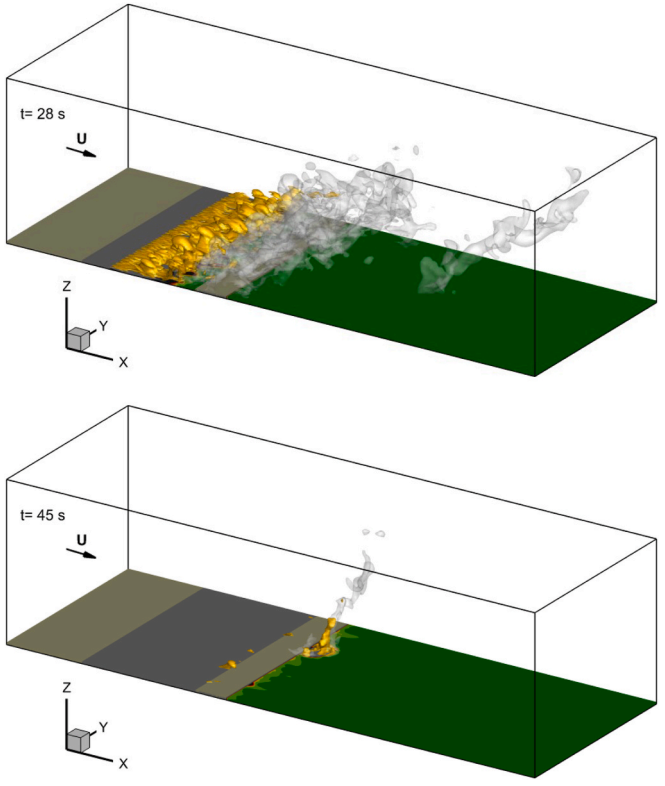

Fig. 10. 3D visualisation of grassland fire obtained for $U_1 = 3$ m s^{-1} and W = 0.5 kg m^{-2} (Nc = 23) as it crosses an 8-m wide fuelbreak. The yellow surface is the isovalue surface T = 1000 K of the gas temperature and the semi-transparent grey surface is the isovalue surface $Y_{H2O} = 10^{-3}$ of the mass fraction of water vapour. (For interpretation of the references to colour in this figure legend, the reader is referred to the Web version of this article.)

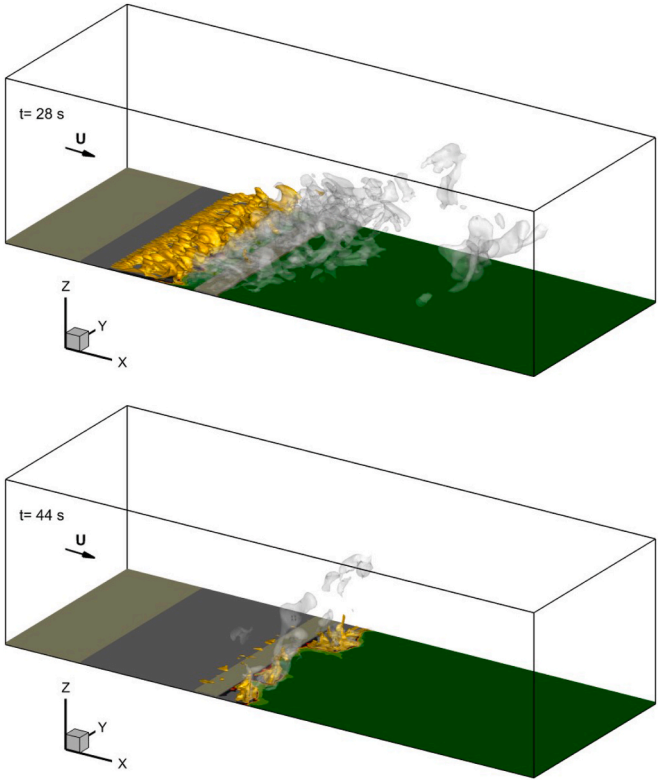

Fig. 11. 3D visualisation of grassland fire obtained for $U_1 = 3$ m s^{-1} and W = 0.5 kg m^{-2} (Nc = 23) as it crosses a 6-m wide fuelbreak. The yellow surface is the isovalue surface T = 1000 K of the gas temperature and the semi-transparent grey surface is the isovalue surface $Y_{H2O} = 10^{-3}$ of the mass fraction of water vapour. (For interpretation of the references to colour in this figure legend, the reader is referred to the Web version of this article.)

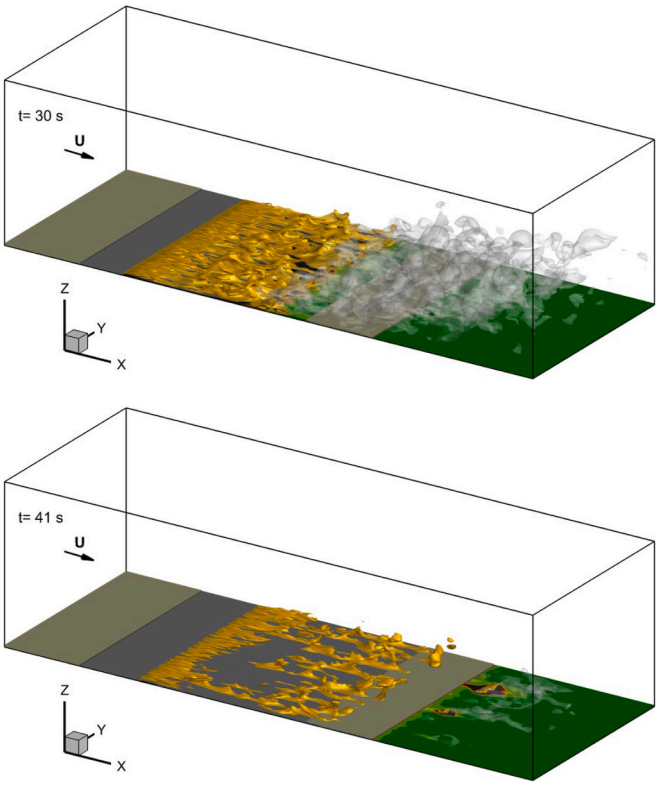

Fig. 12. 3D visualisation of grassland fire obtained for $U_1 = 8$ m s^{-1} and W = 0.35 kg m^{-2} (Nc = 1.95) as it crosses a 17.5-m wide fuelbreak. The yellow surface is the isovalue surface T = 1000 K of the gas temperature and the semi-transparent grey surface is the isovalue surface $Y_{H2O} = 10^{-3}$ of the mass fraction of water vapour. (For interpretation of the references to colour in this figure legend, the reader is referred to the Web version of this article.)

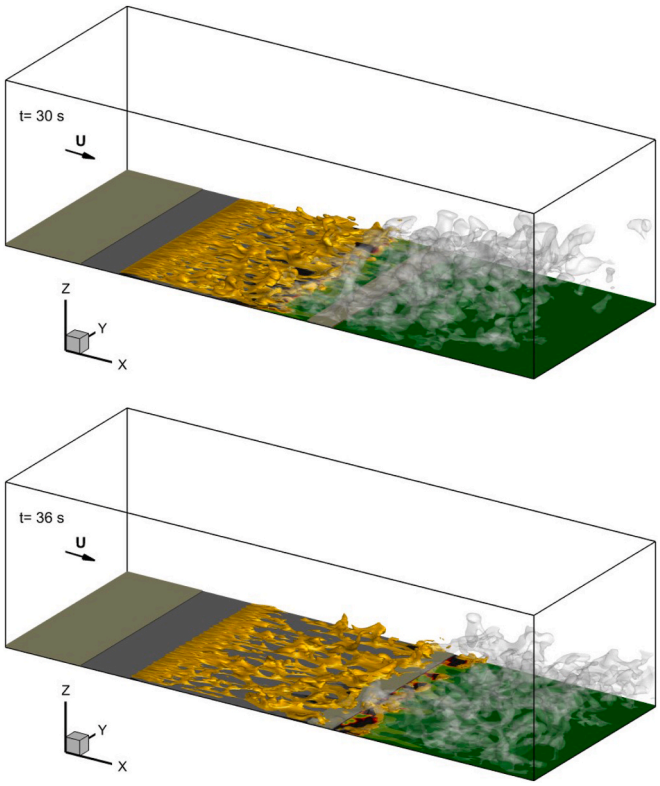

Fig. 13. 3D visualisation of grassland fire obtained for $U_1 = 8$ m s^{-1} and W = 0.35 kg m^{-2} (Nc = 1.95) as it crosses a 6.5-m wide fuelbreak. The yellow surface is the isovalue surface T = 1000 K of the gas temperature and the semi-transparent grey surface is the isovalue surface $Y_{H2O} = 10^{-3}$ of the mass fraction of water vapour. (For interpretation of the references to colour in this figure legend, the reader is referred to the Web version of this article.)

As indicated previously, each configuration (wind speed and fuel load) was tested by introducing several fuelbreak widths, in order to identify the situations for which fire easily crosses, marginally crosses, and does not cross fuelbreak. With this approach, it was possible to determine the extinction limit, L_{FBx}, of fuelbreak width. In order to relate this quantity (L_{FBx}) to other parameters characterizing the fire front, the geometric characteristics of the fire front form in particular the flame height H_F, are extracted from the isotherm surface (T = 1000 K) as shown in Fig. 15. This threshold temperature was chosen as a good compromise in considering that temperature in the flame can vary from 1400 K at the fire front base of to 700 K at the visible tip [40]. Following an idea proposed by Wilson [41], the optimal fuelbreak width (L_{FBx}) is represented in Fig. 16 as a function of fireline intensity I, obtained by dividing the average value of HRR at steady state fire propagation by fire front length L_Y. Based on experimental grassfires and assuming an ignition behind the fuelbreak by direct contact between flames and vegetation, this paper proposed a relationship between the probability for a fire to cross a fuelbreak and the intensity of the incoming fire. The outcome was a linear expression relating these two parameters, given by Eq. (7) [41], where L_{FBx} is expressed in m, I in MW m^{-1}, and P is the probability of fire to cross the fuelbreak.

$$L_{FBx} = \left(\frac{1.36 - A}{0.99}\right) + \frac{0.36}{0.99} I \tag{7a}$$

$$A = Ln\left(\frac{P}{1-P}\right) \tag{7b}$$

Results obtained by numerical simulation, were compared in Fig. 16 with three values of the probability $P = 0.1$, $P = 0.01$, and $P = 0.001$. It can be noted that, except for some particular values, most of the present numerical predictions were located above the values proposed by Wilson [41]. In addition, the slope of the linear-fitting obtained by numerical simulation ($L_{FBx} \sim 0.56 \times I$) is also steeper compared to the empirical expression proposed by Wilson ($L_{FBx} \sim 0.36 \times I$) obtained from Eq. (7a). Various elements could explain these relative discrepancies. First Wilson [41] proposed a criterion exclusively based on the idea that fire crosses the fuelbreak by direct contact between flame and vegetation, ignoring consequently the possibility that heat transfer (by radiation and convection) at a certain distance between flame and vegetation could initiate the ignition of fuel located at the opposite edge of the fuelbreak. Second, one can imagine that the existence of two propagation modes of surface fires (wind-driven and plume-dominated), complicates the existence of a single relationship between optimal fuelbreak width L_{FBx} and fire intensity I. It is precisely for this reason, that an analysis of the present results is proposed by introducing a similitude parameter, Byram's convective number (N_C), able to account for the transition between these two propagation regimes.

In Fig. 16 the numerical results are also compared with the predictions obtained by Eq. (2) from DIMZAL operational model [13,14]. To cover a large range of situations, two threshold heat fluxes $Q_R = 15$ kW m^{-2} and $Q_R = 30$ kW m^{-2} were considered in Eq. (2), as well as two flame tilt-angles: $\gamma = 0°$ and $\gamma = 45°$. These two threshold heat fluxes represent critical values evaluated from classical ignition theory [18–20] using solid fuel properties detailed in Table 1; $Q_R = 30$ kW m^{-2} is the heat flux corresponding to an ignition time equal to 15 s and $Q_R = 15$ kW m^{-2} corresponds to an ignition time equal to 60 s. It must be underlined that the uncertainties about the right heat flux value that must be used to evaluate critical fuelbreak width (L_{FBx}) resulted from the fact that, unlike classical ignition theory, fuel located at the opposite edge of the fuelbreak is not subjected to a continuous heat flux, but to a

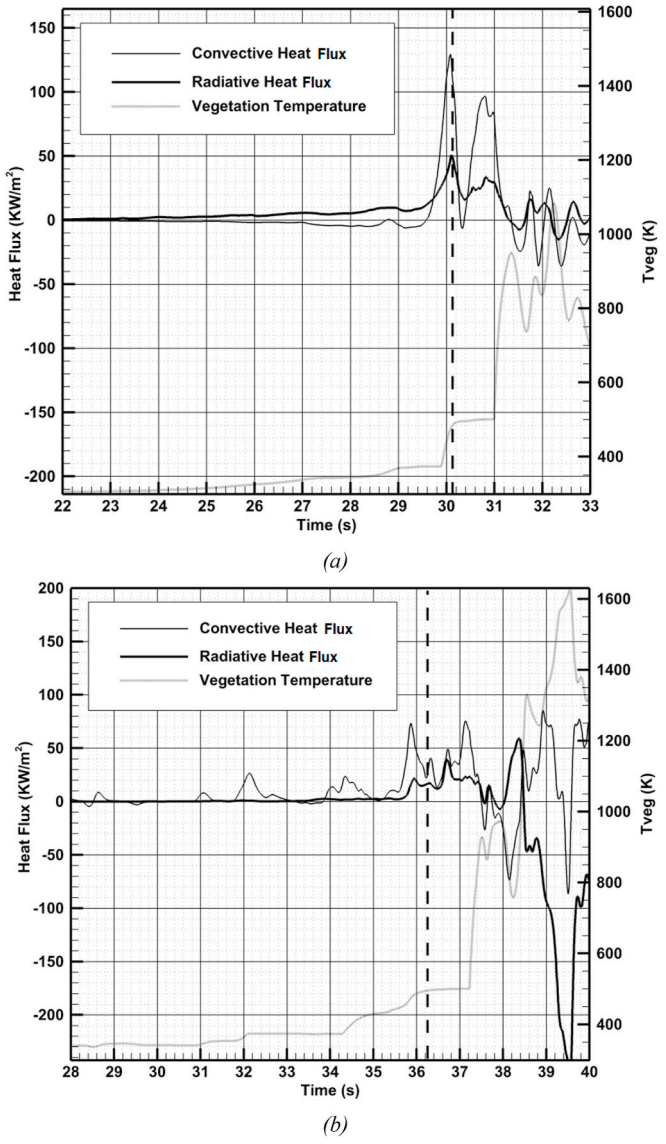

Fig. 14. Time evolution of the convective and the radiative heat fluxes received by a vegetation particle located at the fuel-bed surface and of the corresponding particle temperature, obtained without fuelbreak. (a) $U_1 = 3$ m s^{-1} and W = 0.5 kg m^{-2} (Nc = 23) particle located at point (50 m, $L_Y/2$, H_{Fuel}), (b) $U_1 = 8$ m s^{-1} and W = 0.35 kg m^{-2} (Nc = 1.95) particle located at point (90 m, $L_Y/2$, H_{Fuel}).

time-variable one, because the flame front is not static as it propagates. A second element explaining the difficulty in comparing these two approaches results from the nature of the flame itself: in one case (FIRESTAR3D), the flame is a 3D object (radiating in volume), whereas in the other case (DIMZAL), the flame is assimilated to a 2D radiant panel. Nevertheless, despite these differences, and considering that an operational tool (DIMZAL) must be as simple as possible to be widely used, this comparison is still interesting to improve the degree of confidence associated to the use of the operational tool in practical situations. Fig. 17 directly compares the optimal fuelbreak width evaluated from FIRESTAR3D numerical simulations and from DIMZAL. Unlike the curves shown in Fig. 16 for DIMZAL, in this case the tilt angle was not imposed to an arbitrary defined value (0° and 45°), but was calculated from an estimated ratio between the horizontal component of the gas velocity due to the wind and the vertical component due to buoyancy [22,42]. In this case the best fit (minimizing root square error) was obtained for an incident heat flux equal to 10 kW m^{-2}.

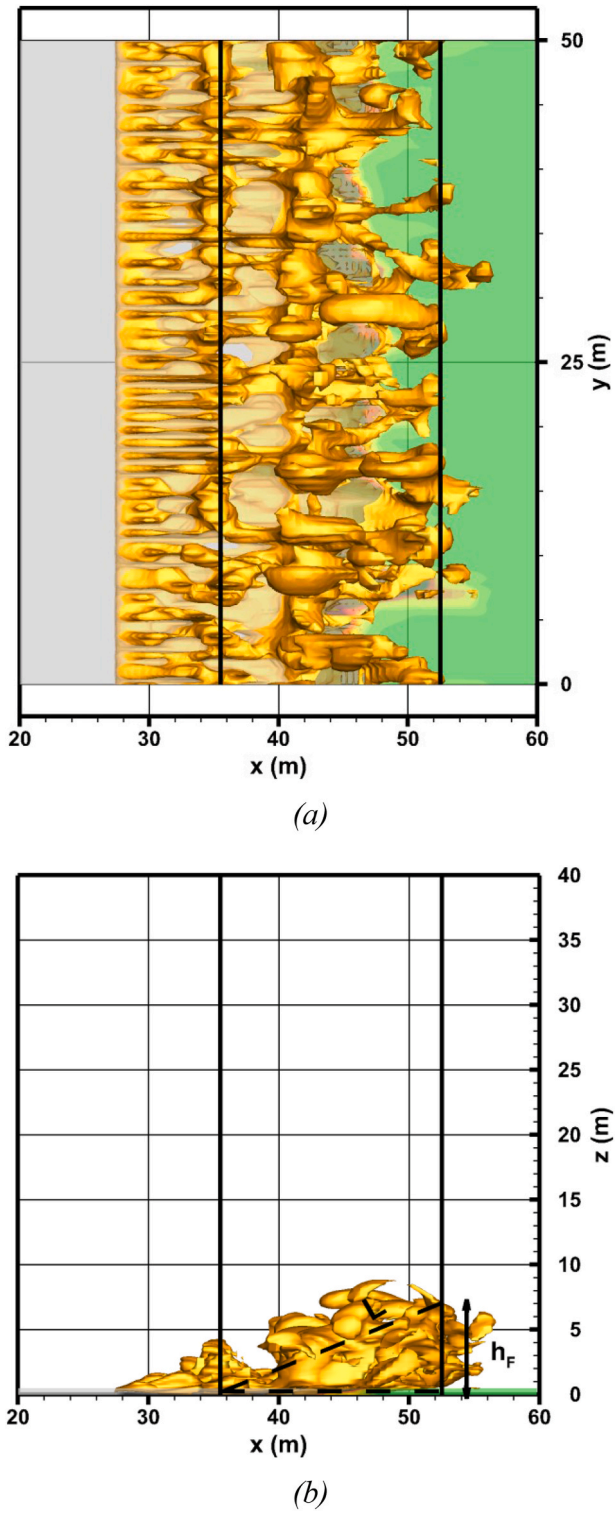

Fig. 15. 3D visualisation of the flame front represented by the isotherm surface (T = 1000 K) obtained for $U_1 = 3$ m s^{-1} and W = 0.5 kg m^{-2} ($N_C = 23$). (a) Top view, (b) lateral view.

The flame height H_F is evaluated graphically as in Fig. 15 and the ratio L_{FBx}/H_F is represented versus Byram's convective number (N_C) in Fig. 18. In comparison with the criterion proposed by Butler and Cohen [15], given by Eq. (3), based on a purely radiative heat transfer calculation, our simulations have shown that critical fuelbreak width was ranged between 1 and 10 times the flame height, depending of fire propagation regime before its arrival at the fuelbreak edge (see Fig. 18).

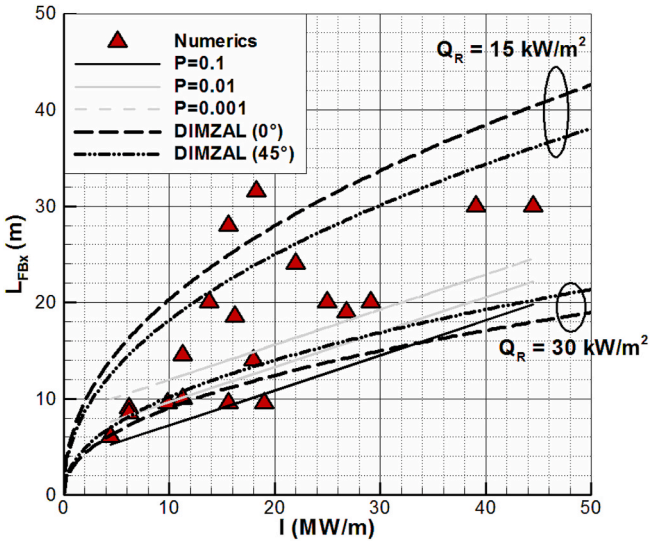

Fig. 16. Optimal fuelbreak width L_{FBx} (lower limit of extinction) versus fireline intensity I. The lines P = 0.1, P = 0.01, and P = 0.001 are obtained using Eq. (7) – the probability for the fire to cross the fuelbreak from Wilson's formula [41], DIMZAL predictions are shown for two flame tilt-angles (0° and 45°) and two critical heat flux values (15 and 30 kW m^{-2}) [13,14].

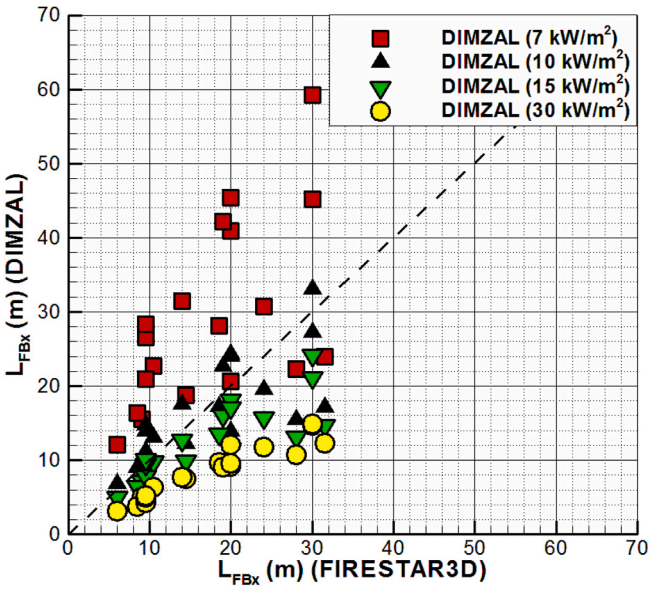

Fig. 17. Optimal fuelbreak width obtained by numerical simulations (FIRESTAR3D) and from DIMZAL operational tool for critical heat flux values (Rossi et al., 2011) [22].

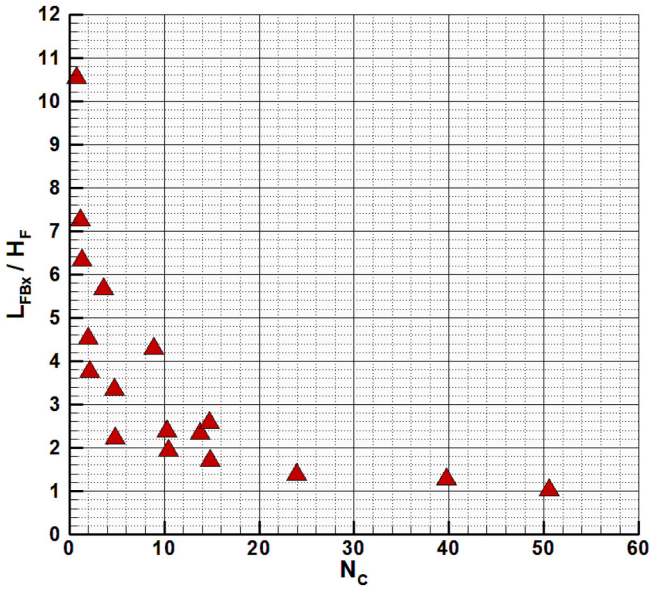

Fig. 18. Optimal fuelbreak width L_{FBx} (lower limit of extinction) scaled by the flame height H_F versus Byram's convective number N_C.

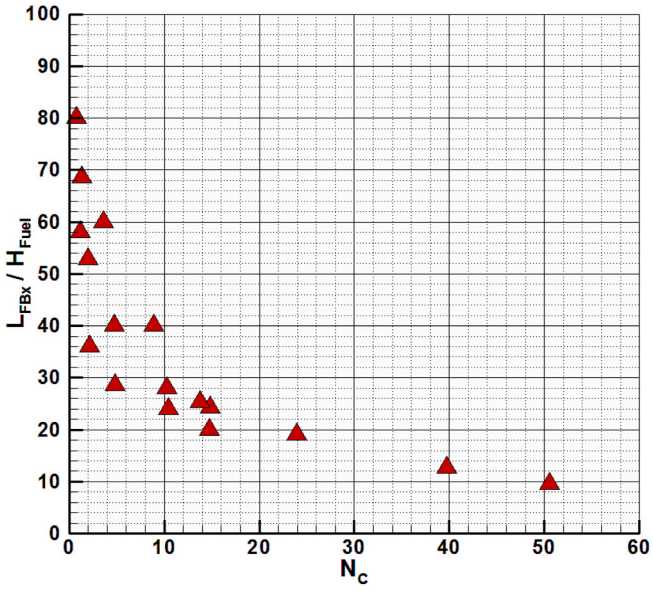

Fig. 19. Optimal fuelbreak width L_{FBx} (lower limit of extinction) scaled by the fuel height H_{Fuel} versus Byram's convective number N_C.

It is not surprising that highest values of L_{FBx}/H_F ratio are obtained for smallest values of Byram's convective number, i.e. for wind-driven fires. This result can be quite easily understood considering that for wind-driven fires, trajectory of the plume can be significantly tilted toward the horizontal by the wind flow allowing hot gases to impact the vegetation layer located behind the fuelbreak, and consequently facilitate its ignition [17]. Same kind of analysis can be done by replacing the flame height (H_F) by the fuel depth (H_{Fuel}), a parameter easier to characterize on the field, and the results are reported in Fig. 19. With this parameter, safety fuelbreak width is ranged between 10 and 80 times the fuel height, for the considered range of Byram's convective number. It is interesting to notice that, even in the worst case, this criterion is in agreement with the recommendation of brushing around houses located in a WUI that varies from 50 to 100 m (this distance is mandatory in WUI in France for example), 100 m is also a typical width for a strategic fuelbreak on both part of a trail used by firefighters.

Whole numerical simulations carried out in this study are summarized in Fig. 20, showing the ratio L_{FB}/H_{Fuel} versus the inverse of Byram's convective number ($1/N_C$). Results were classified in four categories (in increasing safety): "Propagation", "Overshooting", "Marginal", and "No propagation". The difference between the two intermediate categories is the following: in the "Overshooting" situation, fire crosses the fuelbreak with very few ignition points, it propagates over a short distance and then stops; the "Marginal" situation is very similar to "Overshooting" one, but fire behaviour would fall in the "No propagation" category by increasing the fuelbreak width by 1 m. In Fig. 20, small values of $1/N_C$ ($N_C^{-1} < 0.1$) correspond to plume-dominated conditions and larger values of $1/N_C$ ($N_C^{-1} > 0.5$) correspond to wind-driven conditions. This

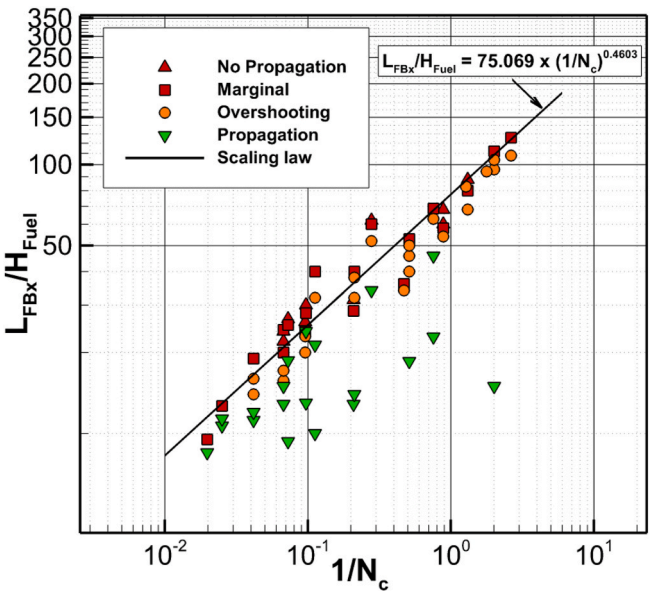

Fig. 20. Effectiveness of a fuelbreak (success and failure): ratio of the fuelbreak width to the fuel height versus the inverse of Byram's convective number.

graph highlights that for very dry grasslands (FMC = 5%) and for the considered range of Byram's convective number, no continuous propagation is observed for L_{FB}/H_{Fuel} larger than 50, spotting with weak propagation and extinction are observed for $L_{FB}/H_{Fuel} < 100$, and $L_{FB}/H_{Fuel} > 100$ the fire would be unable to cross the fuelbreak. The "Overshooting" and "Marginal" data, and consequently the optimal fuelbreak width L_{FBx} (lower limit of extinction), can nicely be fitted by $L_{FBx}/H_{Fuel} = 75.07 \times N_c^{-0.46}$; this law would mark the "Propagation"/"No propagation" transition for the considered range of Byram's convective number. This scaling must however have a limit; logically, the optimal fuelbreak width L_{FBx} cannot increase indefinitely as Byram's convective number decreases. But this limit, if it really exists, could not be reached in the framework of this study.

2. Conclusions

The behaviour of surface fire propagating in grassland with a fuelbreak was studied numerically using a 3D fully physical multiphase model (FIRESTAR3D). 18 combinations of fuel height and wind speed were considered and allowed to cover a large spectrum of fire regimes, from plume-dominated fires to wind-driven fires. Adding fuelbreak width as a variable parameter, a total of 72 simulations were performed. Depending on the ability of fire to cross or not the fuelbreak, the results were classified in four typical categories from "Propagation" to "No propagation", with two intermediate behaviours named "Overshooting" and "Marginal". The ability of fire to successfully cross a fuelbreak depends on its ability to create multiple ignition points behind the fuelbreak that are close enough to have the possibility to merge and to reconstruct a continuous propagating fire front. In the "Overshooting" situation, very few ignition points are created, fire intensity decreases and the fire eventually stops. A "Marginal" case is an "Overshooting" one, but fire behaviour would fall in the "No propagation" category by increasing the fuelbreak width by 1 m. After describing these various behaviours, a more global analysis has highlighted that the critical fuelbreak width significantly increases with fireline intensity (which was expected). By adding Byram's convective number to the analysis, the results have clearly shown that wind-driven fires are much more critical in terms of fuelbreak width (scaled both by the flame height and by the fuel height) compared to plume-dominated fires. This suggests that, in addition to radiation heat transfer, often used to dimension a fuelbreak, convection heat transfer and direct flame contact play an important role in the ability of a fire to cross a fuelbreak. The ratio of optimal fuelbreak width (lower limit of extinction) by fuel height, marking the "Propagation"/"No propagation" transition, could be scaled by a power law with the inverse of Byram's convection number evaluated before fire reaches the fuelbreak. The limit of this scaling law as Byram's convective number decreases could not be reached in the present study. This limit might not exist in practice, because it would correspond to fires propagating in extremely windy conditions for which other effects, such as wind unsteadiness and projected firebrands (burning particles), are likely to play a very important role in the ability of a fire to cross a fuelbreak.

Concerning the effectiveness of fuelbreaks in protecting structures located in WUI, we must keep in mind, that in many situations the main source of vulnerability of houses does not come only from the fire front itself, but from the accumulation of embers particles on the roof or in any place where such particles can accumulate. This fact was confirmed in a post-fire report published after the bushfire that occurred in the region of Canberra (Australia) in January 2003, during which 50% of houses ignitions were due to embers, 35% were due to embers and radiant heat, and only 10% were due to radiant heat alone [43]. Because such firebrands injected in the plume and lifted at high altitudes, can be transported over long distances (several kilometres), this phenomenon must be taken into account in the near future for a more complete safety analysis.

Author statement

Physical and numerical model: Dominique MORVAN, Nicolas FRANGIEH, Gilbert ACCARY. Numerical simulations: Nicolas FRANGIEH, Gilbert ACCARY, Sofiane MERADJI. Preparation of figures: Nicolas FRANGIEH, Gilbert ACCARY: Analysis of numerical results: Dominique MORVAN, Gilbert ACCARY, Jean-Louis ROSSI, Thierry MARCELLI, François CHATELON: Redaction of the paper: Dominique MORVAN, Gilbert ACCARY. Data: Jean-Louis ROSSI, Thierry MARCELLI, François CHATELON. The authors of the following paper.

Declaration of competing interest

The authors declare that they have no known competing financial interests or personal relationships that could have appeared to influence the work reported in this paper.

Acknowledgments

This work was funded by the Corsican Collectivity and the French state in the framework of the collaborative project GOLIAT (CPER: 40031). "Centre de Calcul Intensif d'Aix-Marseille" is acknowledged for granting access to its high-performance computing resources. The authors acknowledge the three reviewers that have allowed to improve the original manuscript.

References

[1] M.A. Moritz, M.E. Morais, L.A. Summerell, J.M. Carlson, J.M. Doyle Wildfires, complexity, and highly optimized tolerance, Proc. Natl. Acad. Sci. U. S. A. 102 (50) (2005) 17912–17917.
[2] K.G. Hirsch, D.L. Martell, A review of initial attack fire crew productivity and effectiveness, Int. J. Wildland Fire 6 (4) (1996) 199–215.
[3] K. Tolhurst, Report on the Physical Nature of the Victorian Fires Occurring on 7th February 2009 Report of the, University of Melbourne, May 2009, p. 18p.
[4] L.R. Green, Fuelbreaks and other fuel modifications for wildland fire control 79p, USDA Agricultural. Handbook, 1977.
[5] J.L. Rossi, D. Morvan, A. Simeoni, Th Marcelli, F.J. Chatelon Fuelbreaks, A part of wildfire prevention, United Nations Office for Disaster Risk Reduction (UNDRR)) (2019), Glob. Assess. Rep. (2019) 25. Geneva, https://www.unisdr.org/we/inform/publications/66111.
[6] J.L. Rossi, B. Komac, M. Migliorini, R. Schwarze, Z. Sigmund, C. Awad, F. J. Chatelon, J.G. Goldammer, Th Marcelli, D. Morvan, A. Simeoni, B, Thiebes Integrating Realistic Societal Behaviour, Shifting from Suppression to Prevention, Raising Awareness, E-STAG Report, 2020, p. 27.

[7] R.B. Hammer, V.C. Radeloff, J.S. Fried, S.I. Stewart, Wildland-urban interface housing during the 1990's in California, Oregon, and Washington, Int. J. Wildland Fire 16 (2007) 255–265.
[8] L.R. Green, H.E. Schimke, guides for fuel-breaks in sierra Nevada mixed-conifer type calif. Forest service, U.S. Dept. Of, in: Agriculture, Pacific Southwest Forest and Range Experiment Station January, vol. 1, 1971, p. 14.
[9] E. Rigolot, M. Costa, in: Conception des coupures de combustible, 2000, p. 90. Cardère Morières, Porto-Vecchio, Corse-du-Sud, France).
[10] J.K. Agee, B. Bahro, M.A. Finney, PhN. Omi, D.B. Sapsis, C.N. Skinner, J.W. Van Wagtendonk, C. Ph Weatherspoon, The use of shaded fuelbreaks in landscape fire management, For. Ecol. Manag. 127 (2000) 55–66.
[11] J.D. Cohen, Relating flame radiation to home ignition using modelling and experimental crown fires Can, J. For. Res. 34 (2004) 1616–1626.
[12] H. Emmons, Fire in the forest, Fire research abstracts and reviews 5 (1964) 163–178.
[13] J.L. Rossi, A. Simeoni, B. Moretti, V, Leroy-Cancellieri an analytical model based on radiative heating for the determination of safety distances for wildland fires, Fire Saf. J. 46 (2011) 520–527.
[14] P.A. Bisgambiglia, J.L. Rossi, R. Franceschini, F.J. Chatelon, L. Rossi, Th Marcelli Dimzal, A software tool to compute acceptable safety distance, Open J. For. 7 (2017) 11–33.
[15] B.W. Butler, J.D. Cohen, Firefighter safety zones: a theoretical model based on radiative heating, Int. J. Wildland Fire 8 (2) (1998) 73–77.
[16] J.L. Dupuy, D. Morvan, Numerical study of a crown fire spreading toward a fuel break using a multiphase physical model, Int. J. Wildland Fire 14 (2005) 141–151.
[17] D. Morvan, Numerical study of the behaviour of a surface fire propagating through a fire break, Fire Saf. J. 71 (2015) 34–48.
[18] D. Drysdale, An Introduction to Fire Dynamics, second ed., John Wiley & Sons, New York, 1998.
[19] P. Reszka, P. Borowiec, T. Steinhaus, J.L. Torero, A methodology for the estimation delay times in forest fire modelling Combust, Flame 159 (2012) 3652–3657.
[20] J.L. Torero, A. Simeoni, Heat and mass transfer in fires: scaling laws, ignition of solid fuels and application to forest fires the Open Thermodynamics, Journal 4 (2010) 145–155.
[21] A. Bar Massada, V.C. Radeloff, S.I. Stewart, Allocating fuel breaks to optimally protect structures in the wildland-urban interface, Int. J. Wildland Fire 20 (2011) 59–68.
[22] J.L. Rossi, A. Simeoni, B. Moretti, V, Leroy-Cancellieri an analytical model based on radiative heating for the determination of safety distances for wildland fires, Fire Saf. J. 46 (8) (2011) 520–527.
[23] D. Morvan, Wind effects, unsteady behaviors, and regimes of propagation of surface fires in open field, Combust. Sci. Technol. 186 (2014) 869–888.
[24] M. Finney, J. Cohen, J. Forthofer, S. McAllister, M. Gollner, D. Gorham, K. Saito, N. Akafuah, B. Adam, J. English, J, Role of buoyant flame dynamics in wildfire spread, Proc. Natl. Acad. Sci. Unit. States Am. 112 (32) (2015) 9833–9838, 2015.
[25] T. Beer, The interaction of wind and fire, Boundary-Layer Meteorol. 54 (1991) 287–308.
[26] N. Frangieh, G. Accary, D. Morvan, S. Meradji, O, Bessonov Wildfires front dynamics: 3D structures and intensity at small and large scales, Combust. Flame 211 (2020) 54–67.
[27] D. Morvan, Physical phenomena and length scales governing the behaviour of wildfires: a case for physical modelling, Fire Technol. 47 (2011) 437–460.
[28] D. Morvan, M. Larini, Modeling of one dimensional fire spread in pine needles with opposing air flow, Combust. Sci. Technol. 164 (2001) 37–64.
[29] K. Gavrilov, G. Accary, D. Morvan, D. Lyubimov, S. Meradji, O. Bessonov, Numerical simulation of coherent structures over plant canopy, Flow, Turbul. Combust. 86 (2011) 89–111.
[30] P. Sagaut Large Eddy Simulation for Incompressible Flows: an Introduction, third ed. Springer, Berlin, Heidelberg, New York.
[31] A.M. Grishin, in: F. Albini (Ed.), Mathematical Modelling of Forest Fires and New Methods of Fighting Them, Publishing House of the Tomsk State University, Tomsk, 1997.
[32] M. Larini, F. Giroud, B. Porterie, J.C. Loraud, A multiphase formulation of fire propagation in heterogeneous combustible, Int. J. Heat Mass Tran. 6–7 (1998) 881–897.
[33] R.R. Linn, A Transport Model for Prediction of Wildfire Behaviour PhD Thesis Los Alamos National Lab, 1997. New Mexico, USA.
[34] D. Morvan, J.L. Dupuy, B. Porterie, M. Larini, Multiphase formulation applied to the modeling of fire spread through a forest fuel bed, Proc. Combust. Inst. 28 (2) (2000) 2803–2809.
[35] D. Morvan, G. Accary, S. Meradji, N. Frangieh, O. Bessonov, A 3D physical model to study the behaviour of vegetation fires at laboratory scale, Fire Saf. J. 101 (2018) 39–52.
[36] N. Frangieh, D. Morvan, S. Meradji, G. Accary, O. Bessonov, Numerical simulation of grassland fires behaviour using an implicit physical multiphase model, Fire Saf. J. 102 (2018) 37–47.
[37] W.E. Mell, S.L. Manzello, A. Maranghides, D. Butry, R.G. Rehm, The wildland-urban interface problem, current approaches and research needs, Int. J. Wildland Fire 19 (2) (2010) 238–251.
[38] D. Morvan, N, Frangieh Wildland convective number and consequences on the regime of propagation, Int. J. Wildland Fire 27 (2018) 636–641.
[39] D. Morvan, S. Méradji, G, Accary Physical modelling of fire spread in Grasslands, Fire Saf. J. 44 (2009) 50–61.
[40] B.M. Wotton, J.S. Gould, W. Lachlan McCaw, N.p. Cheney, S.W. Taylor, Flame temperature and residence time of fires in dry eucalypt forest, Int. J. Wildland Fire 21 (2012) 270–281.
[41] A.A.G. Wilson, Width of firebreak that is necessary to stop grass fires: some field experiments, Can. J. For. Res. 18 (6) (1988) 682–687.
[42] J.H. Balbi, F.J. Chatelon, D. Morvan, J.L. Rossi, Th Marcelli, F. Morandini, A convective-radiative propagation model for wildland fires, Int. J. Wildland Fire 29 (8) (2020) 723–738.
[43] R. Blanchi, J. Leonard, Investigation of Bushfire Attack Mechanisms Resulting in House Loss in the Act Bushfire 2003, Bushfire CRC Report, 2005, p. 61p.